



# Tungsten carbide electrocatalysts prepared from metallic tungsten nanoparticles for efficient hydrogen evolution



S. Emin<sup>a,\*</sup>, C. Altinkaya<sup>b</sup>, A. Semerci<sup>b</sup>, H. Okuyucu<sup>b</sup>, A. Yildiz<sup>b</sup>, P. Stefanov<sup>c</sup>

<sup>a</sup> Materials Research Laboratory, University of Nova Gorica, Slovenia

<sup>b</sup> Faculty of Engineering, Ankara Yildirim Beyazit University, Ankara, Turkey

<sup>c</sup> Institute of General and Inorganic Chemistry, Bulgarian Academy of Sciences, Sofia, 1113, Bulgaria

## ARTICLE INFO

### Keywords:

Tungsten carbide  
Colloid  
Hydrogen evolution  
Overpotential  
Electrocatalyst

## ABSTRACT

Pyrolysis of hexacarbonyl tungsten,  $W(CO)_6$ , in 1-octadecene has been used to prepare colloidal tungsten, W, nanoparticles (NPs). The obtained W NPs has been spin-coated on graphite (C) electrodes. Heat treatment of the W/C electrodes at elevated temperatures ( $\geq 900$  °C) allows the preparation of metallic W and tungsten carbide ( $W_2C@WC$ ) thin films. The obtained  $W_2C@WC$  electrodes were used for hydrogen evolution studies (HER) in 0.5 M  $H_2SO_4$ . Cyclic voltammetry tests for 1000 cycles showed that  $W_2C@WC$  exhibit long term stability without significant drop in current density. The overpotential defined at 10 mA/cm<sup>2</sup> is 310 mV vs. RHE giving an excellent catalytic activity for HER. Materials characterization has been achieved using transmission electron microscopy (TEM), scanning electron microscopy (SEM), and electrochemical impedance spectroscopy (EIS). Here, EIS studies were used to access the charge-transfer resistance of tungsten carbide electrodes.

## 1. Introduction

The process of hydrogen evolution reaction (HER) through water electrolysis is an important technology for establishing the so called "hydrogen economy" [1]. Tungsten carbides are alternative to platinum (Pt) and offer excellent electrocatalytic activity for HER [2–13]. These transition metal carbides found also use in oxygen ( $O_2$ ) reduction reactions (ORR) studies in the form of stand-alone catalysts or as support materials for noble metals like Pt, Pd, Au, etc [14–17]. The high electrocatalytic activity of the two tungsten carbide polymorphs known as  $W_2C$  and WC are ascribed to their *d*-band electronic density states which show similarities with Pt [18–26]. Moreover, tungsten carbides have been demonstrated to be stable both in basic or acidic environments. For example, WC have been used in fuel cells for ORR (basic environment) since it offers superior stability and conductivity compared with commercial carbon known as Vulcan XC-72 [27]. Similarly, WC as a stand-alone catalyst have shown high stability for HER in acidic environment as well [28]. There are number of parameters such as composition, particle size, lattice defects, pseudo-metallic surfaces or the ratio of W/C elements to affect the catalytic activities and stabilities of tungsten carbides [29]. Exploring alternative new methods for synthesis of  $W_2C$  and WC could in principle address some of the holding factors to prepare efficient catalysts.

It has been demonstrated that  $W_2C$  and WC phases can be

synthesized in different ways. For example, one very popular approach for the synthesis of tungsten carbides involves high-temperature reduction of tungsten precursors with carbonaceous gases (e.g.  $CH_4$ ,  $C_2H_2$ , and CO) [30]. The limitation of this method is that at high temperatures uncontrollable particle sintering occurs, giving rise to particles with small surface area. Tungsten carbides can be also synthesized by reacting dicyanide with tungsten-based precursors like ammonium tungstate at 700 °C [31]. Pyrolysis in cage-confinement systems is another way to prepare WC catalysts. This kind of approach avoids sintering of obtained WC NPs during the reaction stage. In this context, Xu et al. have used zeolitic metal azolate framework called MAF-6 to confine a metal source like  $W(CO)_6$  to produce small WC NPs [32]. Pyrolysis of the MAF system at high temperature had resulted in WC nanoclusters with small sizes ca. 2 nm, which have demonstrated excellent electrocatalytic activity for HER with very low overpotential of 51 mV at 10 mA/cm<sup>2</sup>. Reaction of  $WCl_6$  and guanidine hydrochloride at elevated temperatures has been reported to be an interesting approach for synthesis of  $W_2C$  as well [33]. Nitridation of  $WO_3$  with  $NH_3$  at 426 – 726 °C was also found useful to produce intermediate  $\beta$ - $W_2N$ , one step before the end-product  $\beta$ - $W_2C$  [34]. Most of the synthetic approaches for  $W_2C$  and WC uses tungsten precursors where tungsten atom is in high (e.g.  $W^{6+}$ ) oxidation state [35]. So, the literature reports are mainly about reduction of tungsten atom/precursor to lower oxidation state. Currently, there is lack of detailed synthesis of  $W_2C$  and

\* Corresponding author.

E-mail address: [eminsaim@hotmail.com](mailto:eminsaim@hotmail.com) (S. Emin).

WC for HER application where the tungsten precursor is in low oxidation states (e.g. zero) such as metallic tungsten NPs.

Here we used colloidal metallic tungsten (W) NP for the first time to produce  $W_2C$  and WC films on graphite substrate. The procedure uses colloidally stable W NPs which are suited for spin-coating purpose. The approach does not require the use of any oxidative or reducing agents. The graphite substrate acts both as oxidising agent and at the same time it serves as a source for carbon. The synthesis of tungsten carbides occurs at temperatures above 900 °C. While at 1000 °C we obtained mixed  $W_2C@WC$  phases, at higher temperature like 1450 °C we obtained pure WC phase. The prepared tungsten carbide films were found to be efficient electrocatalysts for HER. Material characterization were carried out with X-ray diffraction (XRD), scanning electron microscopy (SEM), transmission electron microscopy (TEM), thermogravimetric analysis, electrochemical voltammetry and electrochemical impedance spectroscopy (EIS).

## 2. Experimental

### 2.1. Materials

Hexacarbonyltungsten (97%,  $W(CO)_6$ ), oleic acid (99%, OA), oleylamine (70%, OLA), 1-octadecene (90%, ODE), chloroform (99.5%,  $CHCl_3$ ), and ethanol (98%, EtOH) were purchased from Alfa Aesar, UK. Graphite block (99.9%) used for electrode preparation was purchased from Beijing Great Wall Co, China.

### 2.2. Synthesis of W nanoparticles

The synthesis of W NPs was carried out under Ar atmosphere at ~230 °C. 1.44 g (4.0 mmol)  $W(CO)_6$ , 0.22 g (2.0 mmol) OA, 1.06 (4.0 mmol) OLA and 25 ml ODE was added in a preheated (130 °C) three-neck flask [36]. The flask was kept at this temperature until  $W(CO)_6$  dissolved. Later, the reaction mixture was gradually heated to 230 °C in 10 min and kept at that temperature for 1 h. The formation of W NPs was evidenced from the color change from transparent to dark. Once the reaction was completed the flask was left to cool to 80 °C A mixture of EtOH: $CHCl_3$  (30:5 ml). was added to the obtained W NPs suspension. Then the suspension was centrifuged at 7000 rpm for 15 min. After decantation 5 ml  $CHCl_3$  was added in the centrifuge tube to dissolve W NPs. The final precipitation was done with 30 ml EtOH. The W NPs suspension was centrifuged. After drying at 40 °C we obtained 0.32 g of W NPs.

### 2.3. Fabrication of $W_2C$ , WC and mixed $W_2C@WC$ electrodes

Fabrication of the textured tungsten carbide thin film electrodes was achieved by spin-coating of W NPs (0.32 g in 2 ml  $CHCl_3$ ) onto graphite substrates and subsequent calcination of the obtained metallic films at 900–1450 °C for 150 min under Ar (99.999%). The suspension of W NPs was prepared by dispersing the obtained W NPs in different volumes of  $CHCl_3$ . For example, we dissolved 0.32 g W NPs in 2 ml  $CHCl_3$  and spin-coated it at 1000 rpm for 20 s. To protect the W NPs from oxidation the tube oven was also loaded with iron turnings which were used as oxygen scavenger.

### 2.4. Characterizations

The morphology of the  $W_2C$  and WC layers was studied with a scanning electron microscope (SEM) (Jeol JSM 7100 F) equipped with a field-emission electron gun and coupled to an energy dispersive X-ray (EDS) spectrometer (Oxford Instruments). Transmission electron microscopy (TEM) studies were carried out with JEOL 2100 F operating at 200 kV. The thermal analysis was conducted with a TGA/DSC 2 system (Mettler Toledo) preset to heating/cooling rate 20 °C/min using nitrogen as a protective (30 mL/min) and purge (40 mL/min) gas in a

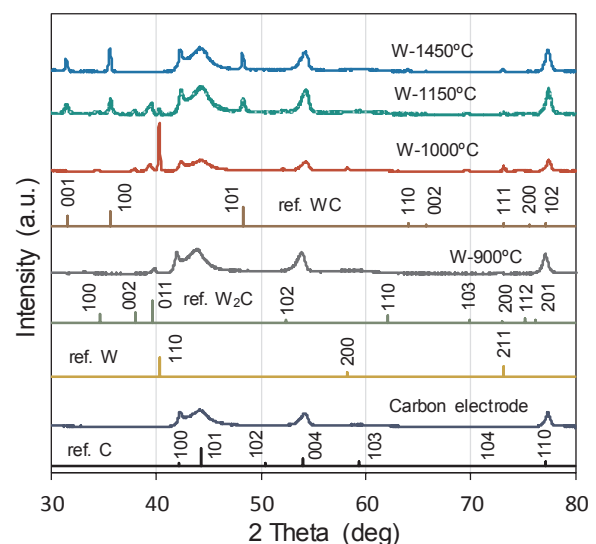


Fig. 1. XRD patterns of W NPs coated graphite electrodes heat treated at 900, 1000, 1150 and 1450 °C. Reference patterns of W,  $W_2C$  and WC are given with labels.

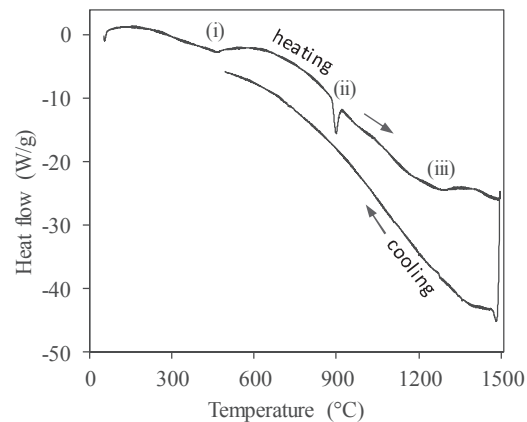
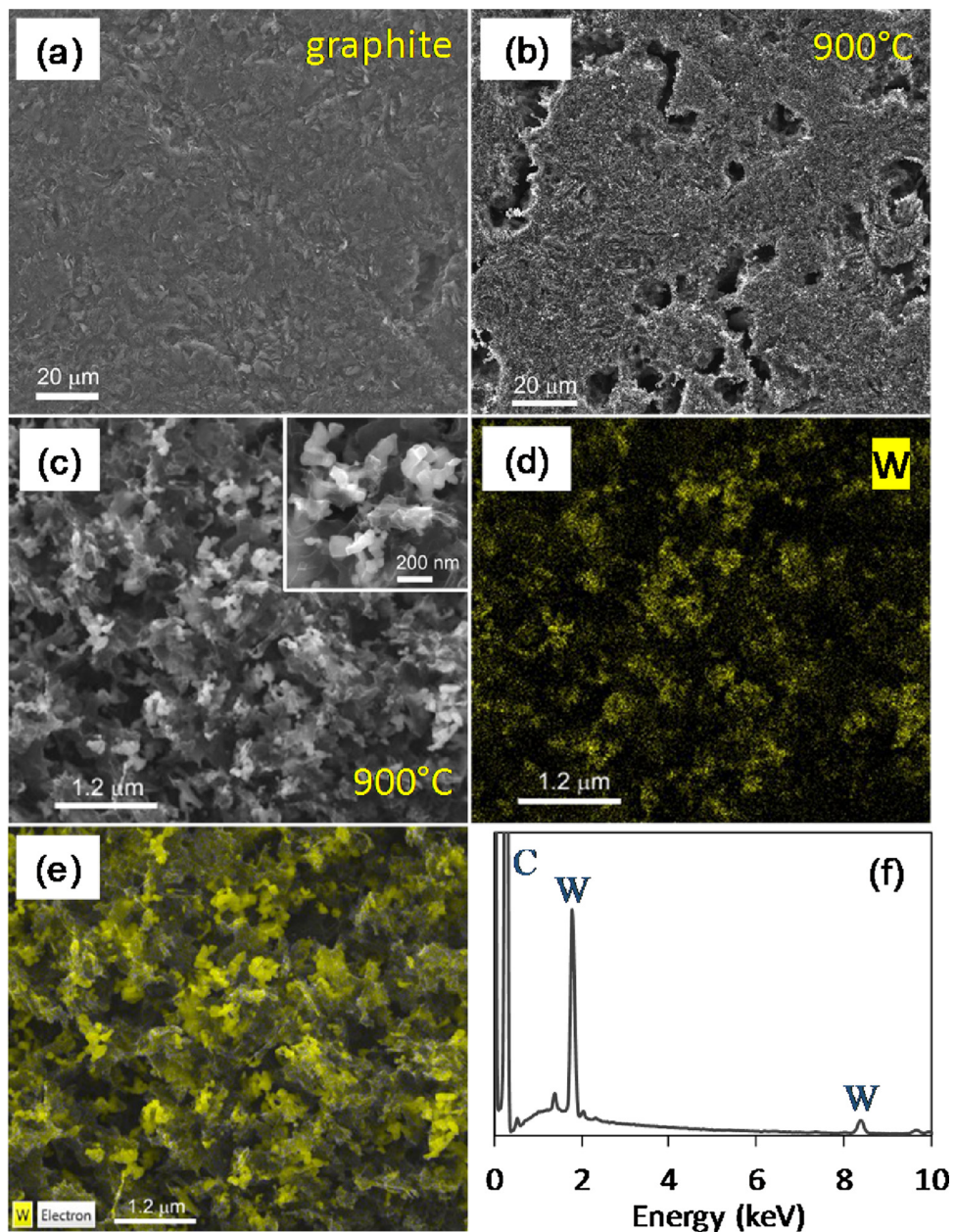


Fig. 2. DSC curves of W sample mixed with carbon recorded with 20 °C/min heating rate under  $N_2$  atmosphere.

70  $\mu$ l alumina (aluminium oxide) crucible covered with a lid. Electrocatalytic measurements were done in a three-electrode configuration in 0.5 M  $H_2SO_4$  aqueous electrolyte solution (pH = 0). The electrochemical cell has an electrode area of 0.283  $cm^2$  defined by an O-ring which is placed between the electrode and the sample holder. The potential of the working electrode was controlled by a potentiostat (EDAQ SP1). A coiled Pt wire (99.999%) and an Ag/AgCl electrode (Sigma-Aldrich) were used as the counter and reference electrodes, respectively. Linear Sweep voltammetry measurements were performed with a scan rate of 2 mV/s. The stability ( $I-t$ ) test was conducted with a graphite counter electrode. The potential values of  $I-V$  data were converted from Ag/AgCl to the reversible hydrogen electrode (RHE) scale according to the following equation:  $E_{RHE} = E_{Ag/AgCl} + E^{\circ}_{Ag/AgCl} + (0.059 \times pH)$  where  $E_{RHE}$  is the calculated potential vs. RHE,  $E_{Ag/AgCl}$  is the measured potential vs. Ag/AgCl and  $E^{\circ}_{Ag/AgCl} = 0.197$  V at 25 °C [37]. The electrochemical impedance spectroscopy measurements were carried out in the 3-electrode configuration in 0.5 M  $H_2SO_4$  at various potential from 0.0 to –0.2 V vs. RHE. The applied frequency range from 10  $\mu$ Hz to 1 MHz with a 10 mV AC dither.



**Fig. 3.** SEM images of (a) pure graphite and (b–e) W NPs coated graphite substrates prepared at 900 °C. In (d–f) are given images with elemental maps for W taken from the object shown in (c). The image in (e) is an overlay of W map with (c). Magnified image of W NPs (white objects) is given as an inset in (c). In (f) is given the spectrum used to construct the maps.

### 3. Results and discussions

#### 3.1. Characterization of the $W_2C@WC$ films

Structural information about the samples heat treated at 900, 1000, 1150 and 1450 °C is presented in Fig. 1. The sample processed at 900 °C shows a small diffraction peak at 40.34° which confirms the presence of metallic W phase (PDF: 9006487). At this temperature the amorphous W phase crystallizes and forms small metallic NPs which sizes ranges between 50 to 300 nm (see below SEM). Further, when the heat treatment is performed at 1000 °C the intensity of the peak at 40.34° increases significantly due to profound crystallization of the metallic W NPs. At 1000 °C it also starts the formation of  $W_2C$  phase (PDF 5910041). If the temperature is raised higher to 1150 °C then evolution of WC phase takes place. The sample heated at 1150 °C contains a mixture of W,  $W_2C$  and WC phases in proportions 9.4:11.4:79.2 wt.% as

estimated using the RIR method [38]. The synthesis of tungsten carbides follows the sequence: W→ $W_2C$ →WC. The formation of tungsten carbides occurs in the presence of metallic W and active carbon ( $C^*$ ) that is produced on the W surface [39]. The diffusion of  $C^*$  into W lattice favours the generation of  $W_2C$  at 1000 °C or WC at 1150 °C. Moreover, pure WC phase has been synthesized at 1450 °C which agrees with a reference WC given in the literature (PDF: 2100636). Fig. 2 shows DSC curves of W sample heated from 50 to 1500 °C under  $N_2$  atmosphere. The sample preparation was done by mixing carbon powder and W NPs. The peak/plateau abbreviated as (i) at around 460 °C accounts for the loss of organic molecules such as stearic acid and oleylamine molecules (capping molecules on W NPs). The next sudden transition abbreviated as (ii) occurs at 900 °C. This peak could be attributed to endothermic reaction like melting of W NPs. Although the melting temperature of bulk tungsten is 3422 °C for W NPs we could expect lower melting points [40]. Moreover, crystalline W NPs has been

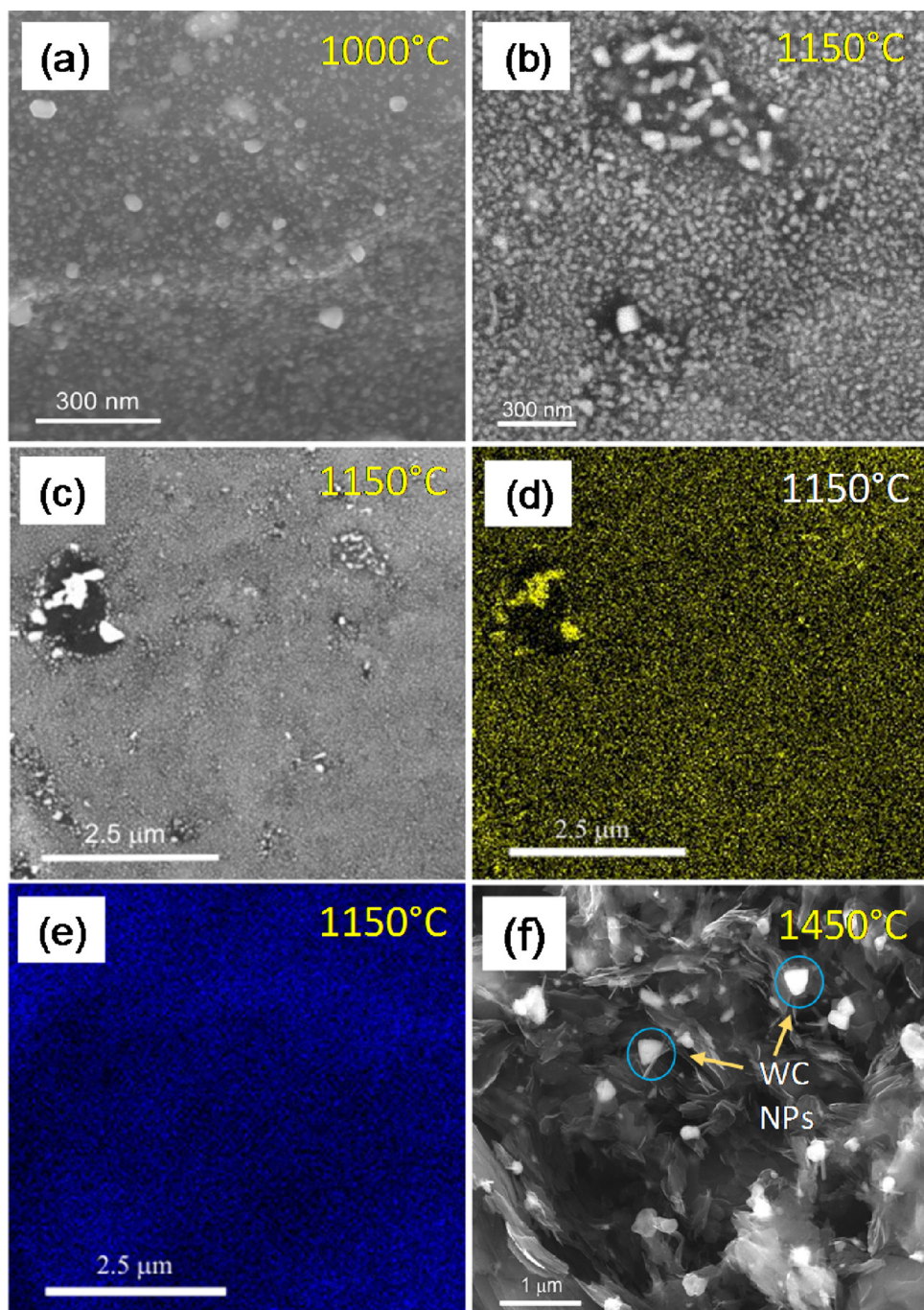


**Fig. 4.** SEM images of W samples heat treated at (a) 1000 °C, (b) 1150 °C, and (f) 1450 °C. In (c) is given an SEM image and elemental maps for (d) W and (e) C of sample prepared at 1150 °C. The scale bars: (a,b) 300 nm, (c–e) 2.5 μm and (f) 1 μm.

observed by XRD (Fig. 1) for the sample heat treated at 900 °C (lowest processing temperature). Crystallization is an exothermic reaction which we do not observe in the DSC curve, but during the continuous heat flow experiment we observe only the endothermic melting reaction of amorphous W NPs. Another peak abbreviated as (iii) in the DSC plot occur at about 1280 °C associated most probably with the formation of tungsten carbide. During the cooling step we do not observe peak for crystallization of W NPs since the metallic W NPs at elevated temperatures reacted irreversibly to WC phase.

Fig. 3 shows SEM images of bare graphite and W NPs coated graphite films heat treated at 900 °C. While the untreated graphite surface is relatively smooth the W NPs coated graphite which was heat treated at 900° shows pores with sizes exceeding > 3 μm in diameter. As sown

in Fig. 3b,c the graphite surface is covered with small W NPs which are in the size range of 50–300 nm. The W NPs in this sample are crystalline as already presented in Fig. 1. The distribution of W on the graphite surface were accessed from the elemental maps obtained from Energy Dispersive Spectroscopy (EDS) studies. Fig. 3d, e shows W map recorded from the object given in (c). An overlay of W map with the SEM image is shown in (e). In the last image the small objects with yellow coloration contain metallic W. Worth mentioning that at 900 °C the sample contain only metallic W NPs without any presence of tungsten carbide phase. From the EDS map we concluded that the W NPs are evenly distributed over the graphite substrate. The EDS spectrum given in Fig. 3i shows signals mainly from C and W elements. Here, the signal of C is unavoidable since the substrate is made of graphite.

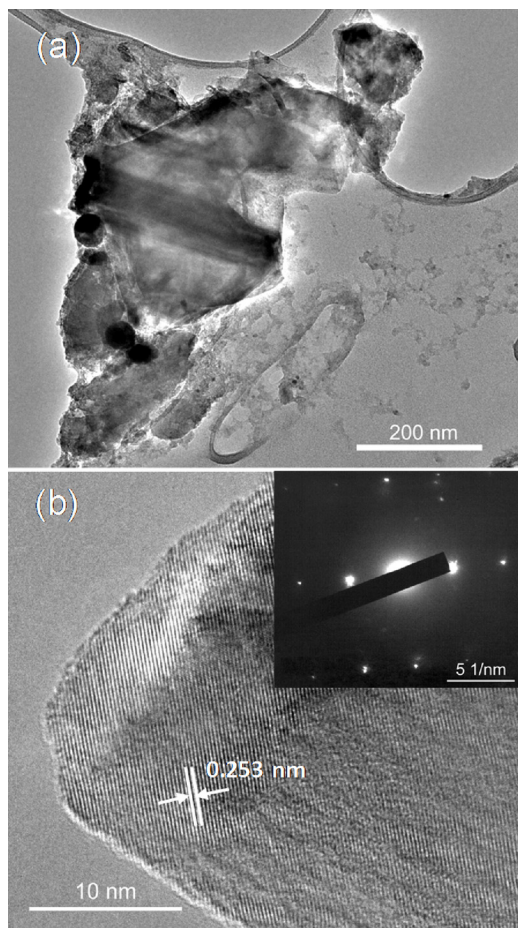


**Fig. 5.** (a,b) TEM image of WC nanosheet at different magnifications. The inset in (b) is an electron diffraction image.

In Fig. 4 are given the SEM images of W samples heat treated at 1000, 1150 and 1450 °C. The W, W<sub>2</sub>C and WC NPs which forms during the heating stage homogeneously cover the surface of the samples. From the SEM images is difficult to define the distribution (e.g. location) of individual W, W<sub>2</sub>C and WC phases. Using EDS we can access only the distribution of W element. In the W1150 °C sample the W element is homogeneously distributed over the graphite (Fig. 4d). On average the size of tungsten-formations increases with the heating temperature. In the sample prepared at 1000 °C the sizes of W-formations range from 40 to 300 nm while those prepared at 1450 °C are much bigger approaching 500 nm. Moreover, the density of WC NPs in the W1450 °C sample is lower due to the larger particle size. Similarly, we can expect that these WC NPs show reduced surface area.

Structural information about the tungsten carbides were obtained from TEM studies. Fig. 5a shows TEM image of WC NP prepared at 1450 °C. The WC phase appear in the form of a nanosheet. We found that the sample is polycrystalline composed of WC crystallites with sizes ranging from several tens to several hundred nanometers (see Supporting Info). Magnified zoom of the WC nanosheet is given in Fig. 5b. The lattice fringes are 0.253 nm which correspond to (100) plane of WC (PDF: 2100636). Moreover, electron diffraction image taken with a selected area aperture confirm the crystal growth along the [100] direction.

### 3.2. Electrocatalytic activity of W<sub>2</sub>C@WC films

The electrocatalytic HER performance of tungsten-based samples recorded in 0.5 M H<sub>2</sub>SO<sub>4</sub> are presented in Fig. 6. As shown in Fig. 6a the lowest potential is obtained with the samples heat treated at 900 °C.

The overpotential for this sample taken at current density of 10 mA cm<sup>-2</sup>, denoted as  $\eta_{10}$ , is 295 mV. For the Pt/C sample which is used as a reference the  $\eta_{10}$  is 110 mV. Moreover, the  $\eta_{10}$  values for a Pt/C catalyst presented in the literature can be as low as ~35 mV [32]. Since, we followed our own protocol for preparation of Pt/C the  $\eta_{10}$  is slightly higher than other reports. The  $\eta_{10}$  for the remaining samples follows the order: W1150 °C–310 mV, W1450 °C–384 mV, and W1000 °C–389 mV. At higher current densities the lowest overpotential at 30 mA/cm<sup>2</sup>, denoted as  $\eta_{30}$ , is obtained with the W1150 °C sample which is 391 mV. On the other side, the  $\eta_{30}$  value of W900 °C sample is 425 mV which makes it less attractive for HER studies. The sample heat treated at 1450 °C which contain phase pure WC produces the lowest current density than the rest tungsten-containing samples.

Another useful metric to interpret the polarization curves is through the comparison of Tafel slope by plotting potential versus  $\log|i|/i$  (current in logarithm) [41,42]. In terms of Volmer limiting step Tafel slope gives illustrative information for the comparison of the kinetic rate of proton discharge reaction:  $H^+ + e^- + M \rightarrow H_{ad} - M$ . As a rule, the lower is the Tafel slope the better is the catalytic performance of the material. Tafel slope of 108 mV/dec for the W1150 °C sample can be assigned to Volmer-Heyrovsky mechanism. The Tafel slopes of the remaining samples are higher and as follows: W900 °C–156 mV/dec, W1000 °C–145 mV/dec, and W1450 °C–143 mV/dec and graphite 162 mV/dec. The lowest Tafel slope of 31 mV/dec is recorded with Pt/C which is due to its high catalytic activity. Chronoamperometric test (*I-t*) of the W1150 °C film was recorded with a graphite counter electrode in 0.5 M H<sub>2</sub>SO<sub>4</sub> (Fig. 6d). The *I-t* test gives a measure of how much stable is the prepared electrocatalyst. Since there is no obvious change of current density (e.g. current) after 3 h test time we can conclude that tungsten carbide material is stable for HER.

To compare our results with the literature data we made a short summary of the overpotentials recorded for tungsten carbide systems (see Table 1). Xu et al., has reported one of the best performing tungsten carbide (WC) catalyst with  $\eta_{10}$ –51 mV [32]. They have shown that small WC NPs (~2 nm) offer this outstanding catalytic performance. The extracted Tafel slope from the polarisation curve is also as low as 49 mV/dec approaching the value ~35 mV/dec reported for their Pt-C catalyst. The trend in Table 1 is very clear, catalysts with high activity for HER exhibit low overpotential and small Tafel slope. Although, the recorded overpotentials by us are higher than the literature reports for the best systems, our study comes useful in showing the relation between synthetic protocol and catalytic activity of materials. Obviously, the best performing systems are made of tungsten carbides with small sizes. In our case, our starting precursor is made of very small (2–4 nm) W NPs. However, during the heat treatment steps these W NPs sinter into larger particles which eventually does not produce catalysts with low (< 100 mV) overpotential. To avoid the sintering of small W NPs into large particles it will require the use of structure confining materials.

Electrochemical impedance spectroscopy (EIS) at different overpotentials was conducted to investigate the underlying electrochemical activity of the synthesized catalysts. Fig. 7 shows Nyquist type plots at different applied potentials. As expected with the increase of overpotential the recorded impedance signal decreases. EIS data were modelled with an equivalent circuit element show in the inset in Fig. 7b. In this model, are used contact phase (CPE) and resistance (R) elements connected in series. The charge transfer-resistance ( $R_{ct}$ ) obtained from the semicircle at low frequencies is related to the kinetics of HER process while the smaller semicircle at high frequencies correspond to ohmic resistance of the medium. The drop of  $R_{ct}$  at high overpotentials is due to faster charge-transfer kinetics (Fig. 7b).

### 4. Conclusions

Our best performing tungsten carbide sample abbreviated as W1150 °C showed  $\eta_{10}$  equal to 310 mV. This sample is a mixture of W,

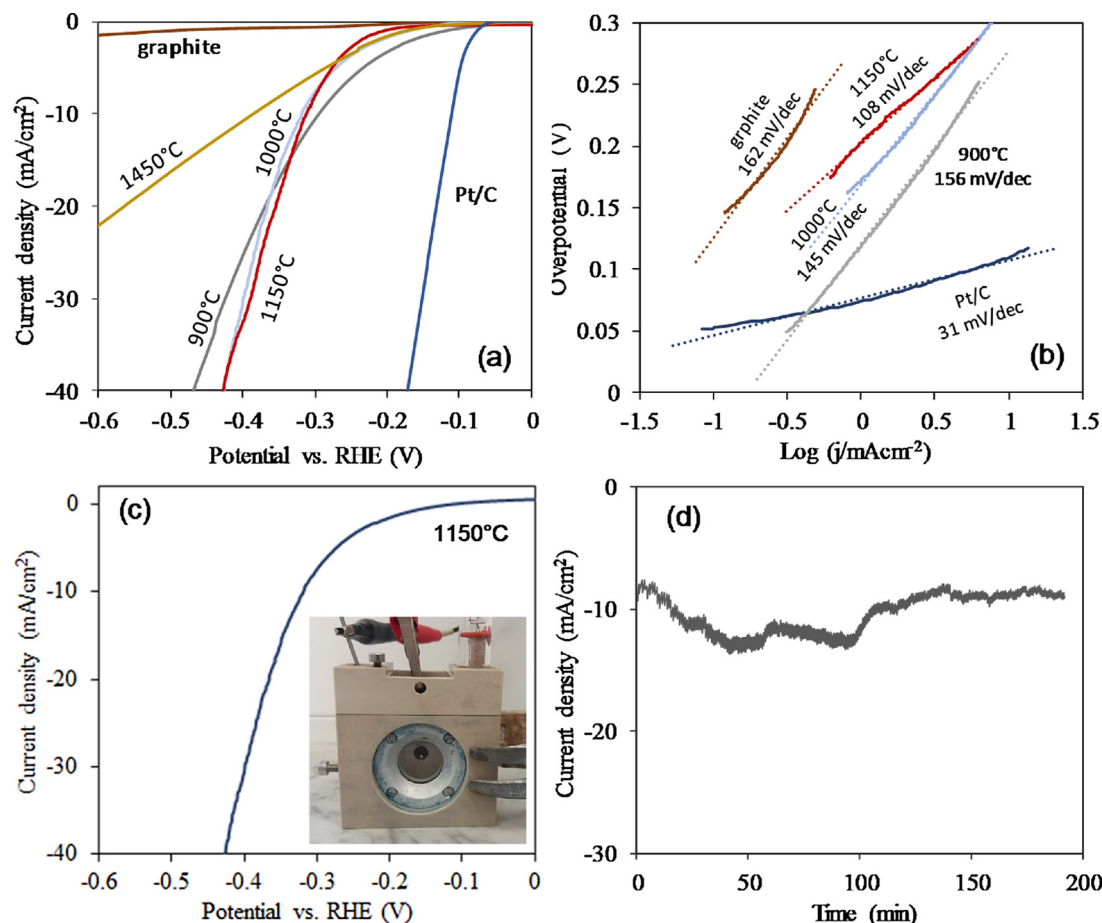


**Fig. 6.** (a) Polarisation curves of W samples heated treated at different temperatures (one compartment cell). The linear sweep voltammograms are recorded in 0.5 M  $\text{H}_2\text{SO}_4$  with a scan rate of 2 mV/s. The reference Pt-C electrode is prepared by coating Pt NPs on graphite. In (b) are given Tafel plots for the different electrodes. (c) Polarisation curves of the sample heat treated at 1150 °C (composition: W:W2C:WC). The inset is a cell used during the tests. In (d) is shown the change of current density vs time ( $I$ - $t$ ) under bias  $-320$  mV in 0.5 M  $\text{H}_2\text{SO}_4$  for the sample prepared at 1150 °C. For the  $I$ - $t$  test a graphite is used as counter electrode.

**Table 1**  
Promising tungsten-based carbides used in HER studies.

Material	Loading (mg/cm <sup>2</sup> )	Tafel slope (mV/dec)	$\eta_{10}$ (mV)	Solution	Ref.
W <sub>2</sub> C NPs (~ 2 nm)	0.209	49	51	0.5 M $\text{H}_2\text{SO}_4$	[32]
W <sub>x</sub> C/graphene oxide NPs	0.14	58.4	100	0.5 M $\text{H}_2\text{SO}_4$	[5]
WC/WN	2.2 – 10	36	105	0.1 M $\text{HClO}_4$	[28]
W <sub>2</sub> C/graphene	2.2	65	120	0.1 M $\text{HClO}_4$	[12]
WC/graphene	0.002	38	120	0.5 M $\text{H}_2\text{SO}_4$	[24]
WC NPs (~ 5 nm)	~ 0.98	84	~ 125	0.5 M $\text{H}_2\text{SO}_4$	[42]
WMoC nanowires	1.28	82	~ 135	0.5 M $\text{H}_2\text{SO}_4$	[10]
WC nanowire	N/A	75	~ 150	0.5 M $\text{H}_2\text{SO}_4$	[7]
WC nanowall	N/A	N/A	160	0.5 M $\text{H}_2\text{SO}_4$	[26]
CoWC	~ 0.28	75 mV	200	0.5 M $\text{H}_2\text{SO}_4$	[31]
WC	~ 0.71	N/A	~ 250	0.5 M $\text{H}_2\text{SO}_4$	[35]
WC <sub>x</sub> /C	1.05	85	264	0.5 M $\text{H}_2\text{SO}_4$	[30]
WC NPs	N/A	122	489	0.05 M $\text{H}_2\text{SO}_4$	[6]
W NPs	~ 2.7	156	295	0.5 M $\text{H}_2\text{SO}_4$	this study
W <sub>2</sub> C/WC NPs	~ 2.7	108	310	0.5 M $\text{H}_2\text{SO}_4$	this study

W<sub>2</sub>C and WC phases. The electrocatalyst has shown good stability during the 1000 cyclic tests. EIS studies has been used to address the charge-transfer resistance ( $R_{ct}$ ) as a function of applied overpotential. The calculated  $R_{ct}$  shows that by increasing overpotential the  $R_{ct}$  value drops. The present strategy offers a convenient way to prepare tungsten carbides films from a solution processed W NPs. One of the main advantages of the current system lies in the W NPs which are stable against coagulation. Spin or spray-coating of W NPs onto various

substrates are among the limitless possibilities to produce evenly coated films.

#### Acknowledgements

This work was supported by the ARRS program (P2-0377) and the bilateral project between Slovenia and China (BI-CN/17-18-021). The authors acknowledge the financial support provided by the Erasmus+

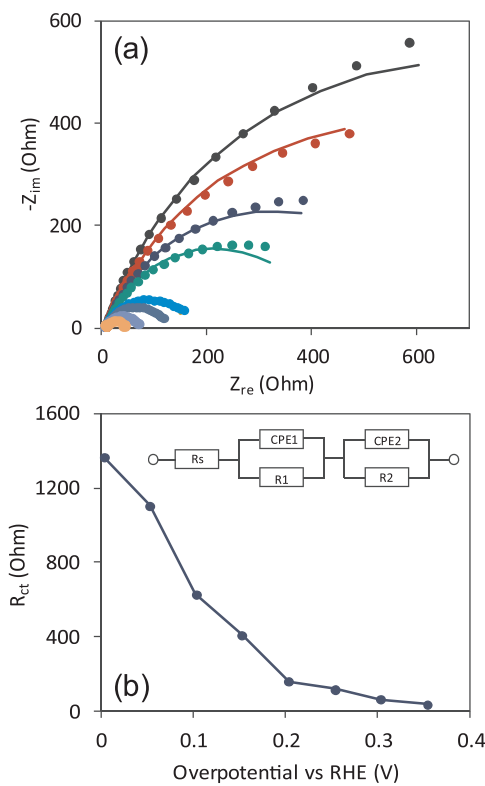


**Fig. 7.** Nyquist plot of W1150 °C in 0.5 M H<sub>2</sub>SO<sub>4</sub> recorded with a bias from 0.0 to 350 mV. In (b) is given the charge-transfer resistance ( $R_{ct}$ ) vs overpotential. The inset in (b) is an electrical equivalent circuit used to fit the EIS data.

program that made it possible for A. Semerci and C. Altinkaya to stay at the University of Nova Gorica.

#### Appendix A. Supplementary data

Supplementary material related to this article can be found, in the online version, at doi: <https://doi.org/10.1016/j.apcatb.2018.05.026>.

#### References

- [1] M.R. Shaner, H.A. Atwater, N.S. Lewis, E.W. McFarland, *Energy Environ. Sci.* 9 (2016) 2354–2371.
- [2] W.F. Chen, J.T. Muckerman, E. Fujita, *Chem. Commun.* 49 (2013) 8896–8909.
- [3] X. Li, X. Hao, A. Abudula, G. Guan, *J. Mater. Chem. A* 4 (2016) 11973–12000.
- [4] X. Zou, Y. Zhang, *Chem. Soc. Rev.* 44 (2015) 5148–5180.
- [5] X.-L. Wang, Y.-J. Tang, W. Huang, C.-H. Liu, L.-Z. Dong, S.-L. Li, Y.-Q. Lan, *ChemSusChem* 10 (11) (2017) 2402–2407.
- [6] J.F. Lin, O. Pitkanen, J. Maklin, R. Puskas, A. Kukuvic, A. Dombovari, G. Toth, K. Kordas, *J. Mater. Chem. A* 3 (2015) 14609–14616.
- [7] X. Fan, H. Zhou, X. Guo, *ACS Nano* 9 (5) (2015) 5125–5134.
- [8] D.J. Ham, R. Ganesan, J.S. Lee, *Int. J. Hydrog. Energy* 33 (2008) 6865–6872.
- [9] H. Zheng, J. Huang, W. Huang, W. Wang, C. Ma, *Electrochem. Commun.* 7 (2005) 1045–1049.
- [10] P. Xiao, X. Ge, H. Wang, Z. Liu, A. Fisher, X. Wang, *Adv. Funct. Mater.* 25 (2015) 1520–1526.
- [11] G. Bianchi, F. Mazza, S. Trasatti, *Z. Phys. Chem.* 226 (1964) 40.
- [12] W.-F. Chen, J.M. Schneider, K. Sasaki, C.-H. Wang, J. Schneider, S. Iyer, Y. Zhu, J.T. Muckerman, E. Fujita, *ChemSusChem* 7 (2014) 2414–2418.
- [13] Z.-Y. Chen, L.-F. Duan, T. Shen, X. Lin, Y.F. Chen, Y.-Q. Chu, S.-G. Sun, W.-F. Lin, Y.F. Chen, Y.-Q. Chu, S.-G. Sun, W.-F. Lin, *ACS Appl. Mater. Interfaces* 9 (2017) 20594–20602.
- [14] H. Meng, P.K. Shen, *Electrochim. Commun.* 8 (2006) 588–594.
- [15] H. Meng, P.K. Shen, *J. Phys. Chem. B* 109 (2005) 22705–22709.
- [16] M. Nie, P. Kang Shen, M. Wu, Z.D. Wei, H. Meng, *J. Power Sources* 162 (2006) 173–176.
- [17] S. Bukola, B. Merzougui, A. Akinpelu, M. Zaema, *Electrochim. Acta* 190 (2016) 1113–1123.
- [18] A.V. Nikiforov, I.M. Petrushina, E. Christiansen, N.V. Alexeev, A.V. Samokhin, *Int. J. Hydrog. Energy* 37 (2012) 18591–18597.
- [19] S. Meyer, A.V. Nikiforov, I.M. Petrushina, K. Köhler, E. Christensen, J.O. Jesen, N.J. Bjerrum, *Int. J. Hydrog. Energy* 40 (2015) 2905–2911.
- [20] P.K. Shen, S. Yin, Z. Li, C. Chen, *Electrochim. Acta* 55 (2010) 7969–7974.
- [21] F. Harnisch, G. Sievers, U. Schröder, *Appl. Catal. B* 89 (2009) 455–458.
- [22] R. Miles, *J. Chem. Technol. Biotechnol.* 30 (1980) 35–43.
- [23] C. Tang, D. Wang, Z. Wu, B. Duan, *Int. J. Hydrog. Energy* 40 (2015) 3229–3237.
- [24] M. Zeng, Y. Chen, J. Li, H. Xue, R.G. Mendes, J. Liu, T. Zhang, M.H. Rümmeli, L. Fu, *Nano Energy* 33 (2017) 356–362.
- [25] A. Eftekhari, *Int. J. Hydrog. Energy* 42 (2017) 11053–11077.
- [26] Y.-J. Ko, J.-M. Cho, I. Kim, D.S. Jeong, K.-S. Lee, J.-K. Park, Y.-J. Baik, H.-J. Choi, W.-S. Lee, *Appl. Catal. B* 203 (2017) 684–691.
- [27] H. Chhina, S. Campbell, O. Kesler, *J. Electrochem. Soc.* 154 (2007) B533–B539.
- [28] F. Meng, E. Hu, L. Zhang, K. Sasaki, *J. Mater. Chem. A* 3 (2015) 18572–18577.
- [29] Z. Chen, M. Qin, P. Chen, B. Jia, Q. He, X. Qu, *Int. J. Hydrog. Energy* 41 (2016) 13005–13013.
- [30] Z.Y. Chen, L.-F. Duan, T. Sheng, X. Lin, Y.-F. Chen, Y.-Q. Chu, S.-G. Sun, W.-F. Lin, *ACS Appl. Mater. Interfaces* 9 (2015) 20594–20602.
- [31] Y. Liu, G.-D. Li, L. Yuan, L. Ge, H. Ding, D. Wang, X. Zou, *Nanoscale* 7 (2015) 3130–3156.
- [32] Y.-T. Xu, X. Xiao, Z.-M. Ye, S. Zhao, R. Shen, C.-T. He, J.-P. Zhang, Y. Li, X.-M. Chen, *J. Am. Chem. Soc.* 139 (2017) 5285–5288.
- [33] S. Decker, A. Lofberg, M. Basin, A. Frennet, *Catal. Lett.* 44 (1997) 229–239.
- [34] F.H. Ribiero, R.A. Dalla Betta, M. Boudart, J. Baumgartner, E. Iglesia, *J. Catal.* 130 (1991) 86–105.
- [35] S.T. Hunt, T. Nimmerwudipong, Y. Roman-Leshkov, *Angew. Chem. Int. Ed.* 53 (2014) 5131–5136.
- [36] S. Emin, M. de Respinis, M. Fanetti, W. Smith, M. Valant, B. Dam, *Appl. Catal. B* 166–167 (2015) 406–412.
- [37] S. Emin, M. Fanetti, F.F. Abdi, D. Lisjak, M. Valant, R. van de Krol, B. Dam, *ACS Appl. Mater. Interfaces* 5 (2013) 1113–1121.
- [38] S. Hillier, *Clay Min.* 35 (2000) 291–302.
- [39] R. Koc, S.K. Kodambaka, *J. Eur. Ceram. Soc.* 20 (2000) 1859–1869.
- [40] A. Moitra, S. Kim, J. Houze, B. Jelinek, S.-G. Kim, S.-J. Park, R.M. German, M.F. Horstemeyer, *J. Phys. D: Appl. Phys.* 41 (2008) 185406.
- [41] Y. Hu, G. Jia, S. Ma, J. Hu, P. Zhu, T. Cui, Z. Li, Z. Zou, *Catal. Today* 6 (208) (2016) 1–9.
- [42] A.T. Garcia-Esparza, D. Cha, Y. Ou, J. Kubota, K. Domen, K. Takanabe, *ChemSusChem* 6 (2013) 168–181.